Collective protection against the type VI secretion system in bacteria

Elisa T. Granato*[1,2], William P. J. Smith* [1,2,3], Kevin R. Foster[1,2]

*Equal contribution

[1] Department of Biology, University of Oxford, Oxford, UK

[2] Department of Biochemistry, University of Oxford, Oxford, UK

[3] Division of Genomics, Infection and Evolution, University of Manchester, UK

ABSTRACT

Bacteria commonly face attacks from other strains using the type VI secretion system (T6SS), a molecular speargun that stabs and intoxicates competitors. Here we show how bacteria can work together to collectively defend themselves against these attacks. This project began with an outreach activity: while developing an online computer game of bacterial warfare, we noticed that one strategist (‘Slimy‘) that made extracellular polymeric substances (EPS) was able to resist attacks from another strategist that employed the T6SS (‘Stabby‘). This observation motivated us to model this scenario more formally, using dedicated agent-based simulations. The model predicts that EPS production can serve as a collective defence mechanism, which protects both producing cells and neighbouring cells that do not make EPS. We then tested our model with a synthetic community that contains a T6SS-wielding attacker (*Acinetobacter baylyi*), and two T6SS-sensitive target strains (*Escherichia coli*) that either secrete EPS, or not. As predicted by our modelling, we find that the production of EPS leads to collective protection against T6SS attacks, where EPS producers protect each other and nearby non-producers. We identify two processes that explain this protection: EPS sharing between cells and a second general mechanism whereby groups of resistant cells shield susceptible cells (‘flank protection’). Our work shows how EPS-producing bacteria can work together to defend themselves from the type VI secretion system.

INTRODUCTION

Bacteria commonly live in densely-populated, multispecies communities where they must compete for limited space and nutrients (1–3). Life in these environments has driven the evolution of an array of bacterial weapon systems, used to inhibit or kill competing microbes (4, 5). One of the most widespread and sophisticated of these weapons is the type VI secretion system (T6SS), a contractile nanomachine that fires a needle into neighbouring bacteria to deliver toxic effector proteins (6).

Possession of the T6SS can confer a strong ecological advantage to bacteria cells (7–10). Conversely, being on the receiving end of a T6SS attack can be lethal. Defending against the T6SS, however, presents a unique set of problems for targeted cells, as—unlike many other weapon systems—the T6SS does not rely on the target cell's surface receptors or transport systems. Instead, it uses mechanical force to pierce the target cell's membrane and deliver its toxic cargo, which limits the potential range of mechanisms that can be employed in defence (11).

In the face of these challenges, here we show how bacteria can work together to protect themselves against T6SS attacks. Individual-level defence mechanisms are known, including immunity proteins, capsule formation, target modification, envelope stress responses, and the removal of susceptibility factors (12–16). However, some of the most powerful defences in bacteria come about when bacteria act as a collective, allowing groups of cells to take advantage of their large numbers (17–22).

This project began when we serendipitously identified a potential collective defence mechanism against the T6SS while developing a video game, as part of an outreach activity. The game—*Gut Wars*—uses an agent-based model developed by our group for research (17, 23–25) to illustrate different bacterial warfare strategies in the human gut microbiome. Running the game repeatedly, we noticed that 'Slimy' strategists, which secrete extracellular polymeric substances (EPS), were particularly resistant against 'Stabby' competitors armed with the T6SS. Secretion of EPS is widespread among bacteria and plays a key role in the formation of biofilms (26, 27). From observation of the game, we hypothesized that EPS released from the cell has the potential to protect both the cell that produces it and others around it, thereby functioning as a powerful collective defence mechanism. There is evidence that EPS has the potential to be physically resistant to T6SSs (12, 13, 15). Moreover, biofilm formation—involving EPS secretion—is known to reduce T6SS susceptibility (14), and is a response to bacterial competition via T6SS (28). We

therefore decided to investigate whether EPS allows bacteria to work collectively in the face of T6SS attacks.

Here, we develop agent-based models of the competitions between T6SS attackers and EPS-producing target cells. As suggested by the computer game, these analyses predict that secreting EPS is a collective defence mechanism in which producer cells both protect each other, and also cross-protect nearby non-producing cells. We test our predictions using a synthetic community, in which T6SS-wielding *Acinetobacter baylyi* are competing with *Escherichia coli* strains secreting free (i.e. non-membrane-bound) EPS in amounts comparable to clinical *E. coli* isolates. These experiments revealed that EPS can indeed serve as a powerful collective defence against T6SS attacks. We identify two processes by which this collective defence can occur: i) EPS sharing between cells and ii) what we call 'flank protection', whereby groups of resistant cells shield non-producers. Interestingly, the latter process appears to be a very general route to collective defence, because it is predicted to occur whatever the underlying mechanism of protection against the T6SS.

RESULTS

Agent-based modelling predicts that EPS can protect against T6SS

Bacteria have evolved a wide repertoire of traits and strategies to increase their survival chances in densely-populated communities. We recently devised a simple browser-based computer game—*Gut Wars*—to showcase some of these competition strategies in a format accessible to children as well as adults. The game asks the user to select different characters representing distinct bacterial competition strategies, which are then pitted against each other in a simulated gut microbiome environment using agent-based modelling (Fig. 1A). Two of the available strategies are EPS production (‘Slimy’) and T6SS firing (‘Stabby’), both common traits in bacteria. While not originally implemented to fulfil this function, we noticed that i) ‘Slimy’ bacteria were surprisingly resistant to T6SS attacks, and ii) the simulated EPS particles covered a large area around the producing cells. This led us to ask whether the secretion of loose (i.e. non-membrane-bound) EPS could protect cells from T6SS firing events, and so help EPS-producing bacteria survive when faced with a T6SS attacker.

To explore these questions, we implemented EPS secretion within an existing individual-based model of T6SS competition (24, 25). Following previous models (29–31), EPS production is

modelled as cells secreting loose, spherical particles into the environment, at a rate P_{EPS} (see Methods). As they grow, divide, and secrete EPS, producing cells create small pockets of EPS particles around themselves, which helps to separate cells from T6SS-wielding competitors (Fig. 1B). Note, we do not assume here that EPS can physically block T6SS needles, as this effect may not be universal (15). However, were this to occur, the expectation is that it will only increase the protection conferred to cells.

We performed simulation parameter sweeps to identify conditions where EPS production was most protective against T6SS attacks. Comparing simulations with and without EPS (respectively, P_{EPS} = 0.1, 0), we used a simple metric to quantify the benefit of EPS protection:

$$\textit{EPS benefit} = (N_{susc}(t_{end}) / N_{susc}(t_{start}))_{EPS+} - (N_{susc}(t_{end}) / N_{susc}(t_{start}))_{EPS-} ,$$

with $N_{susc}(t)$ the number of surviving susceptible cells present at time t. Varying the starting number of attacker and susceptible cells shows that EPS production always offers at least some T6SS protection (*EPS benefit* > *0*), and that production is most beneficial for intermediate attacker- and susceptible cell densities (Fig. 1C).

We performed additional simulations to test the robustness of EPS-mediated T6SS protection with respect to other simulation parameters (Fig. S1). Repeats of competition simulations with different EPS production rates showed that, as might be expected, susceptible survival decreases as the per-cell rate of EPS secretion is reduced (Fig. S1A); below a minimal secretion rate, survival is indistinguishable from that of a non-producing susceptible strain. We also tested a model in which EPS production is costly, such that susceptible cells suffer a growth penalty proportional to their EPS production rate,

$$\textit{Susceptible growth rate} = k_{grow}(1 - c_{EPS}\, P_{EPS}),$$

with k_{grow} the maximum cell growth rate, P_{EPS} the probability of EPS secretion per simulation timestep, and c_{EPS} the unit cost of EPS production. For various $c_{EPS} > 0$, costly EPS production remains net-beneficial to susceptible cells (Fig. S1B), such that the optimal secretion rate $P_{EPS}^* >$ 0. Predictably, EPS investment collapses for excessive costs (Fig. S1B), and is contingent on attacker presence (Fig. S1C). Overall, our simulations predict that production of loose, non-

125 membrane-bound EPS is an effective means for cells to protect themselves against the T6SS,
126 even when costly.

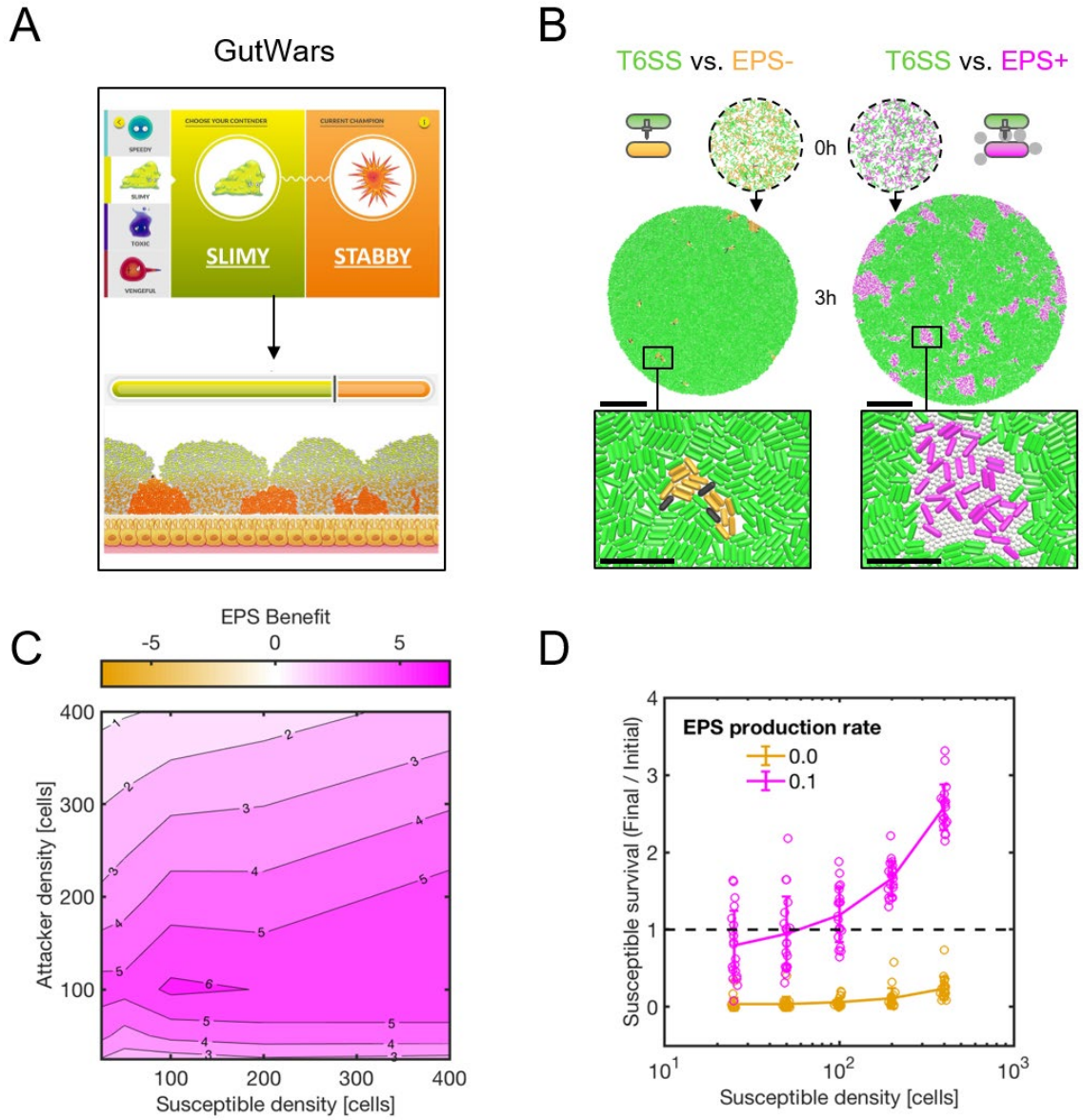

Fig. 1: Agent-based modelling of EPS secretion demonstrates collective defence against the T6SS. **(A)** Snapshots of our agent-based video game 'GutWars', showing EPS-producing 'Slimy' bacteria outcompeting T6SS-armed 'Stabby' rivals. **(B)** Agent-based simulations compete T6SS attackers (green) with EPS non-producing (EPS-, P_{EPS} = 0.0) and EPS-producing (EPS+, P_{EPS} = 0.1) susceptible cells (orange and magenta, right and left columns, respectively). Snapshots show i) initial cell seeding (0h), with 400 cells of each type scattered within a circular homeland, and ii) cell configuration after 3 hours' competition (3h). Scale bars: 50 µm. Zoomed sections highlight dead (black) susceptible cells and distribution of EPS particles. Inset scale bars: 10 µm. **(C)** Contour plot showing measurements of mean EPS benefit (see main text) as a function of initial attacker and susceptible cell density. N=20 simulation replicates per parameter combination. **(D)** Plot showing susceptible final:initial cell counts against initial susceptible density, exemplifying density-dependent benefit of EPS production (fixed attacker density of 400 cells). Individual data points are shown; lines and error bars correspond to data means and standard deviations. Dashed line denotes Final:Initial susceptible ratio = 1, i.e. no net loss or gain of susceptible strain. N=20 simulation replicates per parameter combination; data replotted from (C).

127 **EPS protection is predicted to function as a collective trait**

128 We next used the simulations to more formally evaluate whether EPS protection is a collective
129 trait. A key feature of many collective traits is a positive relationship between the number of
130 individuals with the trait, and the benefit conferred (32). To look for this, we plotted the benefit of
131 EPS production against the starting number of susceptible (EPS producer) cells, which revealed
132 that the relationship is positive for many levels of EPS secretion (Fig. 1D, S2A, S2B). Note that
133 our metric controls for any density-dependent survival effects emerging solely from changes to
134 cell group size (33). That is, while survival is expected to generally increase with susceptible cell
135 number, this effect becomes much stronger when susceptible cells also produce EPS (Fig. 1D).
136
137 Next, we examined the extent to which the benefits from EPS production are shared among cells,
138 which is a second key feature of collective traits. Using the same competition protocol as before,
139 we ran simulations pitting T6SS attackers against susceptible EPS- cells, susceptible EPS+ cells,
140 or both together (Fig. 2A), for a range of initial cell densities. We then quantified the survival of
141 both the EPS+ cells and the EPS- cells when they grew either i) alone with the attacker or ii)
142 paired with the other susceptible cell type (Fig. 2B). As expected when the protective effect of
143 EPS is shared between cells, EPS- survival increased in the presence of EPS+ cells (Fig. 2B,
144 'rescue'), and, conversely, EPS+ survival decreased in the presence of EPS- cells (Fig. 2B,
145 'exploitation').
146
147 **A synthetic community demonstrates collective protection via EPS**

148 To test the model's predictions empirically, we turned to an established experimental system for
149 studying T6SS killing: competitions between a T6SS+ *A. baylyi* attacker strain and a T6SS-
150 susceptible *E. coli* strain (MG1655; (34)). Using their T6SS, *A. baylyi* cells can inject a cocktail of
151 different effector proteins into neighbouring cells which rapidly induce lysis in susceptible *E. coli*
152 (24). To compare the relative T6SS susceptibility of EPS-producing and non-producing *E. coli*,
153 we created *E. coli* MG1655 pRcsA2 (EPS+), a strain capable of undergoing IPTG-inducible
154 production of the exopolysaccharide colanic acid, which is a major component of natural *E. coli*
155 biofilms (35, 36). Colanic acid production is induced via plasmid-based expression of RcsA, the
156 major positive regulator of colanic acid biosynthesis in *E. coli* (37). Its plasmid-free parent
157 MG1655 serves as the non-EPS-producing control strain (EPS-), as MG1655 does not produce
158 significant amounts of colanic acid under the conditions used in this study (Fig. S3).

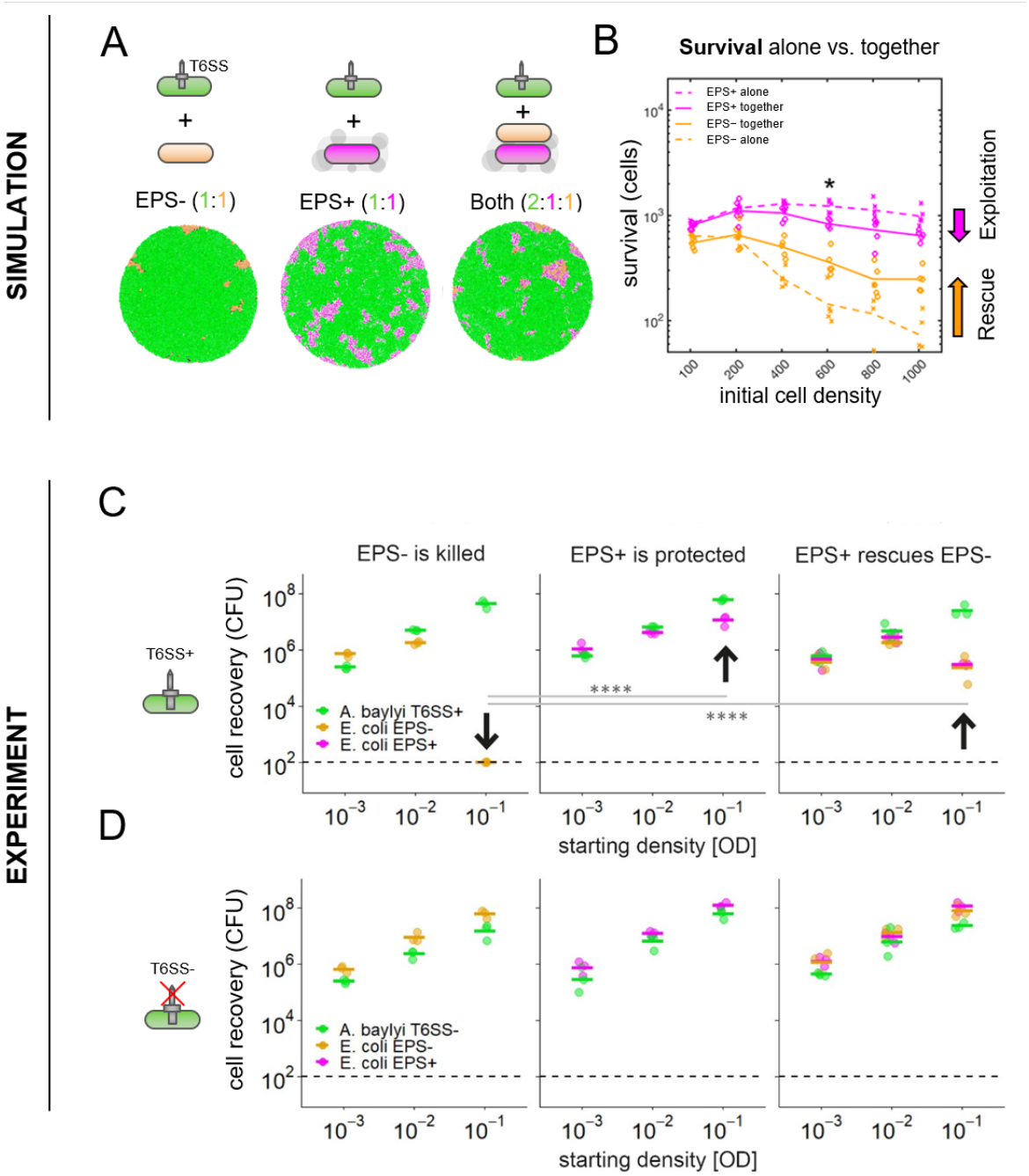

Fig. 2: Modelling and experiments show that EPS secretion protects both producer and non-producer *E. coli* from T6SS attacks. (A) End-state snapshots of agent-based simulations competing T6SS attackers (green) with EPS- or EPS+ (orange, magenta) strains, or both strains at once. **(B)** Survival of each susceptible strain (EPS+, magenta; EPS-, orange) growing alone against T6SS attackers (dashed lines), or together with the other susceptible strain type (solid lines). Asterisk denotes the scenario depicted in (A). **(C+D)** We conducted analogous competition assays *in vitro* between three bacterial strains: *A. baylyi* ADP1 (T6SS attacker), *E. coli* MG1655 Gen^R (EPS-), and *E. coli* MG1655 pRcsA2 (EPS+; colanic acid overproducer). For each strain, cell recovery (CFU) after 6 h of co-culturing at different starting cell densities (optical density; OD) is shown. Individual data points (n=3) and their means are shown as dots and lines, respectively. Arrows highlight key comparisons. **(C)** Survival of *E. coli* EPS- (left), EPS+ (centre) or a 1:1 mix of EPS- and EPS+ (right), when competed against T6SS+ *A.*

baylyi. At high seeding density (OD = 10^{-1}), EPS+ cells survive pairwise competitions against a T6SS attacker better than EPS- cells (centre and left; $p < 0.0001$). When co-cultured with EPS+ and competing against the attacker (right), survival of EPS- cells is strongly increased relative to when they face the attacker alone (left; $p < 0.0001$). When EPS+ cells are co-cultured with EPS- and compete against the attacker (right), EPS+ survival is reduced compared to when they face the attacker alone (left; $p < 0.0001$). **(D)** Repeat of (C) with *A. baylyi* lacking a functional T6SS. When competed against a T6SS- attacker in pairwise competitions, no difference in cell recovery between EPS+ and EPS- cells was detected ($p = 0.66$). For both (C) and (D), competitions were analysed per strain combination and seeding density, with statistical analyses on log-transformed data via two-way ANOVA ($\alpha = 0.01$) with Tukey post-hoc tests (****: $p < 0.0001$).

159 We first sought to measure the amount of colanic acid secreted by the EPS+ strain, as well as
160 test where it is localised with respect to the cell membrane. Across *E. coli* strains, colanic acid
161 can be secreted both as a capsule tethered to the producing cell membrane, as well as in
162 untethered, loose form (38). The difference between these two states is likely to strongly influence
163 the role of colanic acid in collective protection from external assaults. To benchmark our colanic
164 acid quantification and localization assays, we compared the EPS+ and EPS- strains to six clinical
165 *E. coli* isolates (Table S2). As for the majority of the clinical isolates, phase-contrast microscopy
166 showed that our EPS+ strain has no visible membrane-bound capsule. This observation is
167 consistent with colanic acid being untethered from producing cells and released into the
168 extracellular environment (Fig. S3A). This conclusion was further supported by colanic acid
169 quantification assays where we measured the amount of colanic acid found in total cell extracts
170 vs. supernatant fractions of cultures harvested from agar plates. For the EPS+ strain, the entirety
171 of the detected colanic acid was recovered in the supernatant (Fig. S3B). This same assay also
172 revealed that the amount of loose colanic acid secreted by EPS+ is comparable to that secreted
173 by two clinical isolates (#0172 and #0993, Fig. S3B). The EPS+ *E. coli* strain, therefore, secretes
174 loose colanic acid at rates comparable to naturally occurring *E. coli,* allowing for a direct test of
175 the role of EPS in T6SS-mediated competitions.
176
177 Next, we compared the EPS+ and EPS- *E. coli* strains in competition against a T6SS-wielding *A.*
178 *baylyi* (ADP1; T6SS+) and a T6SS-deficient mutant (ADP1 Δ*tssM*; T6SS-). We seeded a 1:1
179 mixture of *A. baylyi* with either EPS+ or EPS- *E. coli* at various densities on agar plates and
180 measured strain recovery after 6 h of co-culture using selective plating (Fig. 2C). At low seeding
181 densities, the T6SS is less efficient because it relies on cell-cell-contact for killing (24, 33). At high
182 seeding densities, we expect the T6SS to be maximally effective; this was confirmed in our
183 competition assays, as the EPS- control strain suffered maximal killing at high densities (Fig. 2C,
184 left). In contrast, the EPS+ strain survived much better at high densities (Fig. 2C, centre), with a
185 10^5-fold increase in survival against T6SS+ *A. baylyi* compared to EPS-. This advantage was

186 dependent on T6SS-activity, as there was no detectable difference in recovery between EPS+
187 and EPS- after pairwise competition with the T6SS- *A. baylyi* (Δ*tssM*) mutant (Fig. 2D). To test
188 whether the presence of EPS in the environment alters T6SS activity, we measured firing rates in
189 hundreds of T6SS+ *A. baylyi* cells exposed to cell-free supernatants with and without EPS, and
190 were unable to detect a difference (Fig. S4). These results strongly support our model's prediction
191 that non-membrane-bound EPS can protect susceptible cells from killing by the T6SS.
192
193 We then examined the potential for a producer strain to cross-protect a non-producer, as expected
194 for a collective defence mechanism. We conducted 3-way competitions between T6SS+ *A. baylyi*
195 and both the EPS+ and EPS- *E. coli* (2:1:1 ratio of *A. baylyi* : EPS+ : EPS-) and quantified strain
196 recovery as above. At high seeding densities, as predicted by the model, the survival of EPS-
197 increased 1000-fold in the presence of EPS+ (Fig. 2C, right) compared to when they faced the
198 T6SS attacker alone (Fig. 2C, left), indicating that the presence of secreted EPS can rescue
199 otherwise susceptible cells from T6SS attacks even if they do not produce EPS themselves.
200 Further consistent with the modelling, we observed that relative survival of the EPS+ strain
201 decreased in presence of EPS- (Fig. 2C, right) compared to when grown alone with the T6SS
202 attacker (Fig. 2C, left) suggesting that the presence of non-producing cells partially compromises
203 the protective effects of EPS production.
204
205 **Cross-protection can emerge from flank protection**
206 Our modelling and experiments show that EPS can function as a collective defence, whose
207 benefit is shared among cells in a colony or biofilm. We next sought to understand the
208 mechanism(s) underpinning this collective property. We initially reasoned that loose EPS would
209 be shared between cells, resulting in the protection of non-producing cells seen in both modelling
210 and experiments. To test this hypothesis, we modified our model so that EPS+ cells no longer
211 secreted loose EPS particles, but instead became intrinsically resistant to T6SS attacks (requiring
212 2 hits to kill instead of 1), as has been demonstrated in capsule-forming bacteria (15). The goal
213 of this model was to remove the possibility of EPS sharing between cells, so that we could test
214 whether sharing was necessary for the cross-protection of non-producer cells (Fig. 3).

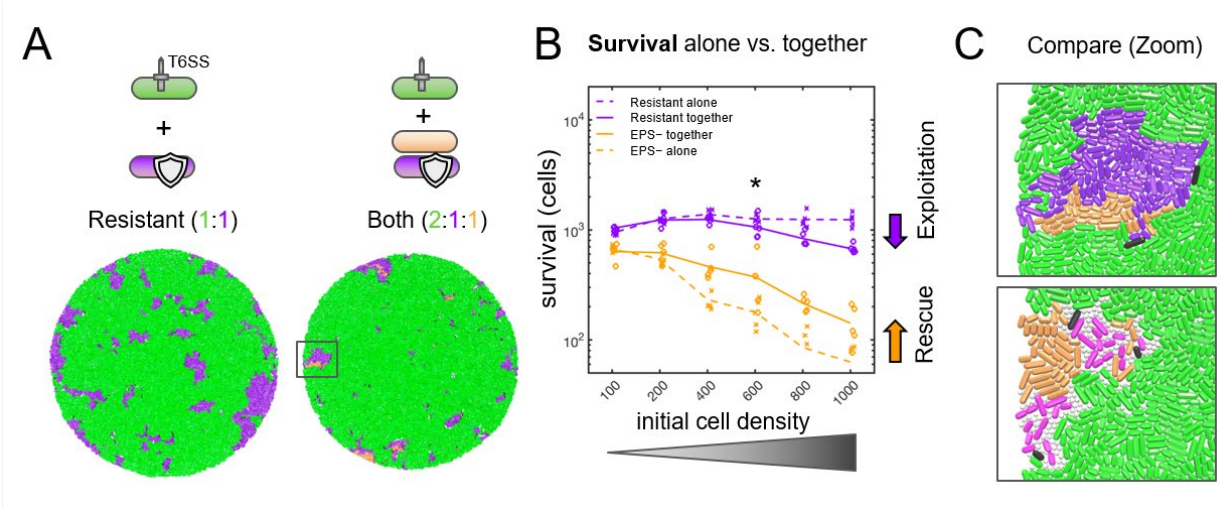

Fig. 3. Modelling shows that cross protection can occur without EPS sharing (A) End-state snapshots of agent-based simulations competing T6SS attackers (green) with an EPS- strain (orange), a T6SS-resistant strain (purple) that secretes no EPS particles, or both strains at once. Box corresponds to zoomed section in (C). **(B)** Survival of Resistant strain (purple) and the EPS- susceptible strain (orange) growing alone against T6SS attackers (dashed lines), or together with the other strain type (solid lines). N=5 simulations per parameter combination; lines denote mean survival. **(C)** Magnified views showing Resistant strain shielding EPS- from the attacker (top), similar to when protection occurs via secretion of loose EPS (bottom).

We then competed the resistant cell type against T6SS attackers as before, either in the presence or absence of the EPS- susceptible cell type (Fig. 3A). To our surprise, this again led to collective T6SS defence, which displayed both cross-protection and the same density-dependence seen for loose EPS (Fig. 3B). Close inspection of simulations revealed that resistant cells act as barriers, protecting the flanks of susceptible cell groups by physically separating them from T6SS attackers (Fig. 3C). We therefore term this mechanism ‘flank protection’. Because it involves one set of cells protecting others, flank protection is also a collective effect, but one that can be provided by a purely private resistance mechanism, as well as by loose EPS.

Time-lapse microscopy reveals both flank protection and EPS sharing

Our modelling raised the possibility that EPS-producing bacteria can collectively defend themselves against T6SS attacks via flank protection, without sharing of EPS between cells. However, an important simplification of the model is that it represents EPS as solid spheres. This limits the ability of EPS to flow past and around cells, restricting sharing in a manner that may not always reflect real EPS (39). We wanted, therefore, to explore both hypotheses—EPS sharing and flank protection—as potential explanations for the collective effects seen in our experiments. To do this, we turned to time-lapse confocal microscopy, which enables direct observation of cells over time (Fig. 4). We competed fluorescent protein-expressing strains of *A. baylyi* (*vipA-sfGFP*,

233 green) with EPS+ *E. coli* (*mScarlet*, magenta) and EPS- *E. coli* (*BFP*, orange) and performed
234 competitions on agar pads as before, except we imaged different locations in the competition area
235 hourly, using confocal microscopy. End-state images of the competition area (Fig. 4A) provided
236 visual confirmation of i) improved survival of EPS+ relative to EPS-, and ii) improved survival of
237 EPS- in the presence of EPS+. Surviving EPS- cells also tended to co-localise with EPS+ cells
238 (bottom right), similar to the behaviour observed in our model.
239
240 To look for signatures of flank protection and EPS sharing, we used automated image analysis to
241 track the movement of boundaries between *A. baylyi* and *E. coli* cell groups in our time-lapse
242 data. We reasoned that, if cross-protection occurs via flank protection (Fig. 4B), we should
243 observe a reduction in the EPS- strain's total exposure to *A. baylyi* attackers. More formally, we
244 should observe a reduction in the length of the interface between *A. baylyi* and EPS- cells, when
245 the EPS+ strain is present, versus when it is absent. Alternatively, if cross-protection occurs via
246 the association of loose EPS with EPS- cells (Fig. 4E), then an EPS- cell group should be able to
247 withstand encounters with the T6SS attacker better when EPS+ producers are present as
248 opposed to absent. Note that the tests we develop are not able to estimate the relative importance
249 of flank protection vs EPS sharing, because the measures used in each test are not directly
250 comparable. Nevertheless, we are able to test whether each play a role in the collective benefits
251 of EPS.
252
253 *Flank protection*: to test for this, we measured the length of *A. baylyi*–EPS- and *A. baylyi*–EPS+
254 group interfaces over time (see Methods). We compared competitions where the susceptible
255 strains grew alone alongside the attacker with those where both susceptible strains were present.
256 To account for the greater initial abundance of EPS- cells in the former case (2:2 *A. baylyi :* EPS-
257 ratio instead of 2:1:1 *A. baylyi :* EPS- : EPS+), we normalised boundary measurements by the
258 initial relative abundance of each *E. coli* strain (that is, dividing interface lengths by 2 for *E. coli*
259 strains growing alone). As we further discuss in the methods, this normalisation is likely to provide
260 a conservative test of whether flank protection is contributing to cross-protection in experiments
261 (see Methods). Shown in Fig. 4C, these normalised measurements confirm that EPS- indeed has
262 reduced exposure to the attacker when co-cultured with EPS+ ('together') vs. without ('alone'),
263 with the improvement being most pronounced between hours 3 and 4 of competition. Comparing
264 the total attacker exposure (area under curves in Fig. 4C) of each susceptible strain grown alone
265 or together, alongside analogous measurements for T6SS- controls (Fig. 4D), we find that the
266 presence of EPS+ significantly reduces EPS- exposure to *A. baylyi*, consistent with the flank

protection hypothesis. Conversely, EPS+ exposure changes only marginally in the presence of EPS-, which is consistent with the inability of the EPS- strain to effectively shield the flanks of EPS+ groups.

EPS sharing: to assess this, we measured the rate of *A. baylyi* encroachment into EPS+ and EPS- cell groups (Fig. 4E), normalising this by the total length of interface between *A. baylyi* and each individual susceptible strain (see Methods). The resulting metric, which we term the normalised invasion rate, provides an estimate of how susceptible each *E. coli* strain is to T6SS attack. Crucially, since the normalised invasion rate examines *A. baylyi*–EPS+ and *A. baylyi*–EPS- strain interactions separately, it excludes any possible effects of flank protection. Measurements of normalised invasion rates over time showed that the EPS- strain was indeed invaded less rapidly when grown together with the EPS+ strain, vs. when grown alone (Fig. 4F, left). Meanwhile, the EPS+ strain was invaded at a consistently lower rate (Fig. 4F, right) than the EPS- strain, with normalised invasion rates largely unchanged by the presence / absence of the EPS- strain (i.e., no significant exploitation effect detected). Importantly, this variation was contingent on T6SS activity: control experiments showed minimal variation in EPS- strain invasion with EPS+ strain presence when attackers lacked a functional T6SS (Fig. 4G, right).

In conclusion, our analyses suggest that both processes—flank protection and EPS sharing—contribute to the collective benefits of EPS in the face of T6SS attackers.

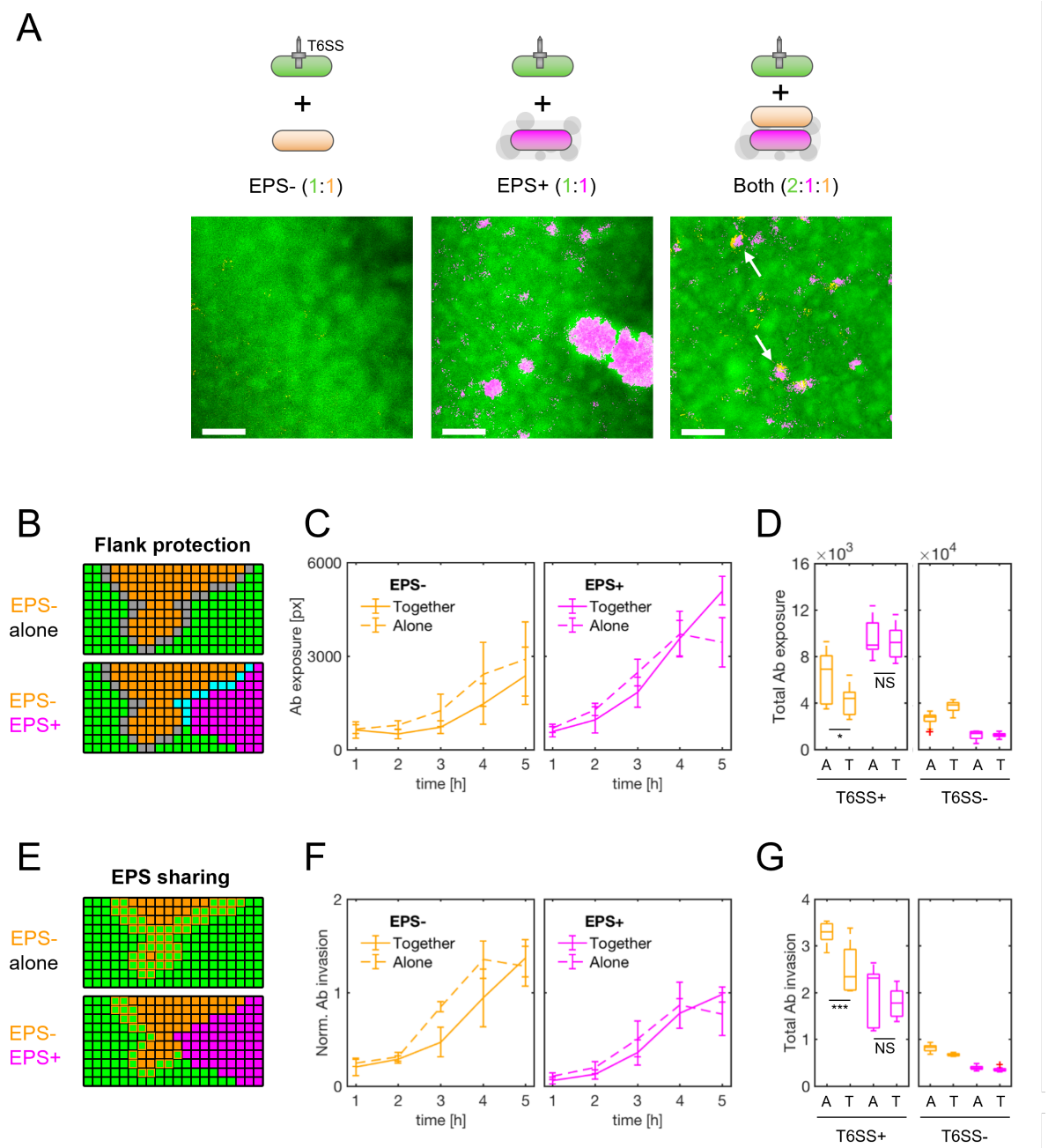

Fig. 4: Timelapse microscopy shows that EPS producers cross-protect non-producers via both flank protection and EPS sharing. (A) *A. baylyi* attacker (green), EPS- (orange) and EPS+ (magenta) *E. coli* strains expressing fluorescent proteins were mixed and co-cultured as before (Fig. 2C,D), this time analysing competition dynamics using confocal microscopy. Colonies were imaged for 7 h at 1 h intervals, across five 470 x 470 µm frames spanning the colony edge (position 1) to its centre (position 5). Example images shown are zoomed-in areas of interest from position 4 (t = 6 h); scale bars: 50 µm. **(B)** Automated image analysis to identify flank protection: when the EPS- strain is cultured alone (top), its exposure to the attacker (grey boundary) is greater than when the EPS+ strain is occluding part of the EPS- group flank (bottom, cyan boundary). **(C)** Time plots of *A. baylyi* exposure for EPS- (left) and EPS+ (right) strains, grown alone (dashed lines) or together (solid lines), and normalised by initial relative abundance. (**D**) Comparison of total normalised exposure (area under curves in (D)) across all strain pairings, including T6SS- controls. 'A' and 'T' denote 'Alone', 'Together'. **(E)** Automated image analysis to identify signatures of EPS sharing: when the EPS- strain is cultured alone (top), it is invaded more

rapidly by the attacker than when EPS+ is present (bottom), consistent with EPS being shared between *E. coli* strains. **(F)** and **(G):** as with (C, D) but now measuring *A. baylyi* invasion rates, normalised by boundary length. In (C,D,F,G), lines connect data means, and error bars denote standard deviations. Time-lapse data was aggregated over colony positions 2-5; position 1 was excluded for analysis since cells quickly grew beyond a monolayer, confounding our 2-D analysis. N=3 biological replicates; 12 data points per time point. Red crosses denote outlier data points ($<$ Q1 - 1.5 * IQR or $>$ Q3 + 1.5 * IQR). Significance assessed using one-sample Kruskal-Wallis tests: * denotes $p = 0.0327$; *** denotes $p = 0.0004$; N.S., non-significant ($p > 0.05$).

DISCUSSION

The production of EPS is a defining property of bacterial biofilms, where the majority of bacteria spend their lives (27). A key challenge for bacteria living in biofilms is the potential for exclusion by competing strains and species (4). Our modelling shows how EPS production can help with this challenge by allowing bacteria to work together and protect themselves against armed competitors. Moreover, an experimental test of our model revealed that EPS dramatically increases *E. coli* survival in competition with T6SS-wielding *A. baylyi*. Here, colanic acid is secreted into the extracellular environment and we find evidence that it has the potential to protect cells other than the producer. Secretion of colanic acid is widespread in *Enterobacteriaceae* such as *E. coli*, *Klebsiella*, *Salmonella* and *Enterobacter* (40, 41), where it plays an important role in biofilm formation (35, 36, 42), and confers protection against various environmental stressors such as desiccation, osmotic stress, and oxidative stress (43, 44). Moreover, elevated EPS production (mucoidy) readily evolves in *E. coli* and other species in response to predation by phages (45–47), and membrane-anchored capsules can protect pathogenic bacteria from attacks by the immune system (48–50). EPS-mediated protection from T6SS attacks could therefore also evolve as a by-product of adaptation to other types of stressors, as well as a direct response to T6SS attacks itself.

Both our modelling and experiments showed that EPS non-producing cells are able to survive T6SS attacks better when co-cultured with EPS producers. Our initial hypothesis was that this cross-protection stemmed from the sharing of loose EPS between EPS producers and non-producers. Unexpectedly however, our simulations identified a second cross-protection mechanism, whereby groups of T6SS-resistant producers reduced the exposure of non-producers to attackers (flank protection). We turned to image analysis of our experimental system to examine these possibilities, which suggested that both flank protection and EPS sharing are important in practice. Interestingly, the role we find for EPS secretion implies that secreted EPS can shield non-producing cells, at a range spanning multiple cell lengths, in a manner not seen in the model. However, this finding does not necessarily imply that EPS has evolved *to be shared*

with non-producers: it is possible that cross-protection of nearby non-producing cells is a by-product of a diffusible molecule evolved to be shared between cells of the same EPS-producing genotype. Indeed, social evolution theory predicts that such interactions are more likely accidents than evolved altruism (31, 51, 52).

Overall, our findings suggest that EPS production—widespread among bacteria—will frequently result in collective resistance to T6SS attacks, including in cases where EPS is not shared between cells (15). Flank protection in particular has the potential to be highly general: it is predicted to emerge whenever sensitive cell groups interface with resistant cell groups, without assuming anything about the underlying resistance mechanism. Flank protection, therefore, has the potential to be mediated by other mechanisms of T6SS resistance, such as envelope stress responses (13, 16), or the production of immunity proteins (14). Indeed, we hypothesise that flank protection has the potential to occur against any contact-dependent weapon, including against the T4SS, T7SS, and Cdi (contact-dependent growth inhibition) systems (4), adding further complexity to interbacterial interactions. Such effects underline the potential for third parties to weaken interactions between bacterial strains in diverse communities. This idea is known from the study of bacterial cooperation, whereby the presence of other species can limit the potential for cooperating strains to work together ('social insulation') (52, 53).

T6SS-wielding bacteria are increasingly being considered as potential biotherapeutics, capable of delivering toxins into pathogenic bacteria (54, 55). Our work cautions that many species have the potential to resist such attacks due to the widespread ability of bacteria to work as collectives. Consistent with this, bacteria are already known to display collective defences against antibiotics (17, 19, 22), predators (56) and phage (20), and biofilm formation continues to be a major issue in industry and medicine (57–60). Strategies that seek to remove problem strains, therefore, needs to consider the ability of bacteria to work both as individuals and as groups.

MATERIALS AND METHODS

Agent-based modelling

We ran agent-based model simulations using the open-source modelling software Cellmodeller (61). To simulate T6SS-mediated interactions and EPS particle secretion, we devised additional code modules, available for download at https://github.com/WilliamPJSmith/CellModeller. The key processes incorporated in our model are summarised here.

349 Model description

350 *Cell growth and division*. Bacterial cells are modelled as exponentially-growing, rigid elastic rods
351 with fixed radius R, which push on one another as they elongate and divide (after doubling their
352 initial volume V_0, plus a small random noise term η_{div}). All cells are assumed to have equal access
353 to growth-limiting nutrients. Generally, cells pay no growth penalty for using either T6SS needles
354 or EPS secretion, and so a cell's volume V increases over time as $\Delta V = k_{grow} V \Delta t$, with k_{grow} the
355 maximum specific growth rate, and Δt the simulation timestep. However, we also explored
356 scenarios in which EPS secretion carried a range of growth costs proportional to the EPS
357 secretion rate (see Fig. S2B,C). Immediately after cell growth, an energy penalty method is
358 applied each timestep to compute cell movements necessary to minimise total cell-cell overlap,
359 subject to viscous drag forces acting on each cell. This process, described previously in detail
360 (23, 61), approximates the elastic repulsion forces acting between cells in physical contact.

361 *EPS secretion*. Similar to previous work, we model agglomerations of EPS polymers as inert,
362 pseudospherical particles (29–31). EPS+ cells secrete these particles from randomly chosen
363 points on their surface. These particles have radius 0.4 μm, rod segment length 0.01 μm, and are
364 assumed mechanically identical to bacterial cells. The secretion probability per time step, P_{EPS}, is
365 at most 0.1, such that the max secretion rate is capped at 1 particle per timestep. EPS particles
366 persist indefinitely, and completely ignore the effects of T6SS toxin injection (see below).

367 *T6SS interactions*. Each time step, T6SS+ cells can fire needles of length $R/2$, projecting
368 orthogonally from randomly chosen sites on their cell surface. The number of firings per cell per
369 unit time is drawn from a Poisson distribution, whose mean is k_{fire}. After firing, each needle is
370 checked to determine if it comes into contact with any other cell in the population (line-segment
371 method). Subsequent to this contact finding, each cell's state is updated to indicate the number
372 of T6SS needle hits it sustained. Cells die (cease growing) after being struck N_{hits} times in this
373 way, and lyse (disappear) following a fixed delay of $1 / k_{lysis}$. Each T6SS needle can deliver its
374 toxin payload to at most one cell. T6SS+ cells are assumed completely immune to their own T6SS
375 toxins, such that they effectively ignore all collateral fire from clone-mates. EPS particles do not
376 obstruct T6SS needles, and so EPS particles can only protect bacterial cells from T6SS attacks
377 by enforcing spatial separation of attacker and susceptible cells.

378

379 Computation and post-processing

380 All agent-based simulations were run using a 2017 Apple MacBook Pro laptop computer, with
381 concurrent simulations distributed between an Intel 3.1 GHz quadcore i7-7920HQ CPU, an Intel

382 HD 630 Graphics card, and an AMD Radeon Pro 560 Compute Engine. Simulation data were
383 visualised using Paraview software, and analysed using custom Matlab and R scripts.
384
385 Simulation protocols
386 All simulations were initialised by randomly scattering different combinations of cells on a flat
387 surface, within a circular 'homeland' of radius 50 μm. At simulation time t = 0, all cells lie flat on
388 the surface, but have randomised orientations. All simulations were run for 130 time steps (Δt =
389 0.025 h), totalling 3.25 h of simulated time. Depending on conditions (most crucially, the number
390 of EPS particles present), most simulations had a runtime of between 10 and 30 minutes
391 (approximately 10 simulations per hour after concurrency).
392
393 **Bacterial growth conditions**
394 All strains were routinely grown overnight in 5 ml LB medium (per L: 10g Tryptone, 10g NaCl, 5g
395 Yeast Extract) in 15 mL polypropylene tubes with agitation (220 rpm). Where necessary, the
396 medium was supplemented with streptomycin (50 μg/mL), ampicillin (100 μg/mL), carbenicillin
397 (100 μg/mL) or gentamycin (15 μg/mL). Routine culturing was carried out on 1.5% w/v LB Agar
398 at 37°C (*E. coli*) or 30°C (*A. baylyi*). All pre-cultures and experiments were carried out at 30°C on
399 0.8% w/v LB Agar, unless indicated otherwise. Optical density (OD) of liquid cultures was
400 measured at 600 nm. For time-lapse microscopy experiments, samples were kept at 30°C
401 throughout the duration of the experiment using a custom-built incubation chamber.
402
403 **Strain construction**
404 For the generation of MG1655 *mScarlet-I*::Tn7 and MG1655 *mTagBFP2*::Tn7, MG1655 cells were
405 transformed with either pGRG25-P*max*::*mScarlet-I* or pGRG25-P*max*::*mTagBFP2* via
406 electroporation and selected on ampicillin at 30°C. The resulting transformants were cultured for
407 16 h at 30°C in liquid LB medium supplemented with ampicillin and arabinose (0.5% w/v). A small
408 volume (appr. 5 μL) of these cultures was streaked onto 1.5% w/v LB agar supplemented with
409 arabinose (0.5% w/v) and incubated at 42°C for 12 h. For each construct, three fluorescent
410 colonies were then selected, streaked onto 1.5% w/v LB agar and incubated at 42°C for 12 h.
411 Resulting colonies were tested for ampicillin sensitivity. For the generation of *E. coli* MG1655
412 *mScarlet-I*::Tn7 pRcsA2, MG1655 *mScarlet-I*::Tn7 cells were transformed with pRcsA2 (37) via
413 electroporation and selected on 100 μg/mL carbenicillin at 37°C. All plasmids and strains used in
414 this study are listed in Table S2.
415

416 **Competition assays**

417 To monitor survival of different *E. coli* strains in competition with *A. baylyi* strains, overnight
418 cultures of *A. baylyi* and *E. coli* were diluted (*A. baylyi* 1:10; *E. coli* 1:100) into 5 mL of fresh LB
419 medium supplemented with appropriate antibiotics (Table S2) and 0.5 mM IPTG to induce
420 production of colanic acid. We used *vipA-sfGFP*-labelled *A. baylyi* ADP1 as the T6SS-positive
421 competitor, whereas an isogenic *tssM* deletion mutant was used as T6SS-negative control
422 competitor. Cultures were then grown for 3 h with agitation, washed twice with LB medium, and
423 resuspended and normalized in LB medium to an optical density at 600 nm (OD600) of 0.1. An
424 *A. baylyi* strain was then mixed with an *E. coli* strain at a ratio of 1:1 (100 µL : 100 µL), and for
425 each strain combination 5 µL were spotted in triplicates in 24-well plates pre-filled with LB agar
426 supplemented with 0.5 mM IPTG (1 mL per well). For experiments at different seeding densities
427 (Fig. 2), the initial 1:1 mix was further diluted 10-fold (for OD = 0.01) or 100-fold (for OD = 0.001)
428 before being spotted on LB agar. For experiments with three competitors (Fig. 2), one *A. baylyi*
429 strain and two *E. coli* strains were normalized to OD = 0.1, mixed at a ratio of 2:1:1 (*A. baylyi* : *E.*
430 *coli* : *E. coli*), and further diluted if required before being spotted on LB agar. Plates were then
431 dried in a laminar flow at room temperature for approximately 20 min to allow droplet drying,
432 before being incubated at 30°C for 6 h. After incubation, competition spots were washed off with
433 500 µL NaCl (0.8%) each and subjected to seven rounds of 10-fold serial dilution. Colony-forming
434 units (CFUs) of *A. baylyi* and *E. coli* strains were determined by plating on streptomycin (100
435 µg/mL; selecting for *A. baylyi*), ampicillin/carbenicillin (100 µg/mL; selecting for *E. coli* MG1655
436 pRcsA2) or gentamycin (15 µg/mL; selecting for *E. coli* MG1655 Gen^R) media, incubated at 30°C
437 (*A. baylyi*) or 37°C (*E. coli*).

438

439 **Determination of T6SS firing rate**

440 To determine T6SS firing rate in *A. baylyi* cells exposed to EPS produced by *E. coli* (Fig. S4A),
441 cells of *E. coli* EPS+ and EPS- were grown overnight for 16 h at 37°C, and 1 mL of bacterial
442 suspension was centrifuged for 5 min at 17000 g to sediment cells. The resulting supernatants
443 were sterile-filtered using 0.2 µm syringe filters (Sartorius), and 5 µL were each pipetted onto
444 separate cut-outs (ca. 5 mm x 5 mm) of 1% w/v LB agarose and left to dry for 20 min at room
445 temperature. In parallel, cells of the focal strain (*A. baylyi* T6SS+ *clpV-mCherry2*) were grown to
446 exponential phase in liquid culture (OD600 ~ 0.8-1.0) before spotting 1 µL of culture onto the
447 agarose pads treated with supernatant, and leaving them to dry for 5 min at room temperature.
448 Pads were then inverted onto a 5-cm diameter glass bottom Petri dish with a 3-cm diameter
449 uncoated n° 1.5 glass window (MatTek Corporation), so that the cells were sandwiched between

450 the agarose and the glass. The sample was then moved to the microscope and imaged
451 immediately. Time-lapse fluorescence microscopy was performed using a Zeiss Axio Observer
452 inverted microscope with a Zeiss Plan-Apochromat 63x oil immersion objective (NA = 1.4) and
453 ZEN Blue software (version 1.1.2.0). Time-lapse images were recorded for 3 minutes at a 10-
454 second interval. Exposure times were 1.05 ms for brightfield and 500 ms for mCherry2 (ex:
455 589 nm | em: 610 nm). The rate of T6SS firing was measured in a total of n = 916 *A. baylyi* cells
456 via detection of ClpV (*mCherry*) fluorescent foci (24). Each new ClpV focus was assumed to mark
457 one T6SS contraction event in a focal cell. Three separate fields of view at different locations on
458 the same agarose pad were monitored for each treatment. Image analysis was performed using
459 FIJI 2.1.0/1.53c (62). For each field of view, total number of cells and ClpV foci were determined
460 each minute via thresholding, segmentation and object counting in the brightfield channel, and
461 the FIJI built-in 'Find maxima' function in the mCherry fluorescence channel, respectively
462
463 **Colanic acid quantification**
464 To quantify the amount of colanic acid (CA) produced by different *E. coli* strains (Fig. S2), 1 mL
465 of overnight cultures were washed once with fresh LB medium and density-adjusted to an OD of
466 1.0. For each strain, 50 µL were then spotted in triplicates in 24-well plates pre-filled with LB agar
467 supplemented with 0.5 mM IPTG (1 mL per well). Plates were then dried in a laminar flow at room
468 temperature for approximately 20 min to allow droplet evaporation, before being incubated at
469 30°C for 6 h. Cell material was then harvested by adding 1 mL of sterile ddH_2O to the well and
470 pipetting up and down until all material was suspended, and then transferred to a sterile 1.5 mL
471 tube. Tubes were vortexed for 5-7 seconds, and the OD600 was determined for all replicates. Of
472 these volumes, twice 400 µL were then transferred to two separate reaction tubes pre-filled with
473 600 µL ddH_2O: one for quantification of total CA, and one for quantification of CA secreted into
474 the extracellular environment. For quantification of total CA (Fig. S3), samples were boiled for 20
475 min at 95°C, centrifuged at 17'000 g for 20 min, and 1 mL of supernatant was used for further
476 processing. For quantification of CA in the extracellular environment (Fig. S3), samples were
477 centrifuged at 17'000 g for 20 min, and 1 mL of supernatant was used for further processing. To
478 test whether sterile-filtering removes EPS from supernatants (Fig. S4B), *E. coli* MG1655 pRcsA2
479 (EPS+) and MG1655 Gen^R (EPS-) strains were grown overnight for 16 h at 37°C, and 1 mL of
480 bacterial suspension was centrifuged for 5 min at 17000 g to sediment cells. The resulting
481 supernatants were either sterile-filtered using 0.2 µm syringe filters (Sartorius) or left unfiltered,
482 and 900uL of supernatant was used for further processing. Relative CA production was then
483 determined through the quantification of L-Fucose (63). Briefly, samples were boiled with 4.5 mL

484 $H_2SO_4 \cdot H_2O$ (6:1 H_2SO_4 and H_2O) for 20 min and cooled to room temperature. Then, 900 µL of
485 each sample was transferred to a spectrophotometer cuvette and absorbance was measured at
486 396 nm (A_{396}) and 427 nm (A_{427}). To each cuvette was then added 100 µL of freshly prepared L-
487 cysteine hydrochloride (1M), mixed by pipetting, and absorbance was again measured at 396 nm
488 (A-cy_{396}) and 427 nm (A-cy_{427}). The concentration of L-Fucose was then determined by calculating
489 (A-cy_{396} − A_{396}) − (A-cy_{427} − (A_{427}) and applying a previously generated L-Fucose standard
490 curve (0-100 µg/mL).
491
492 **Confocal microscopy**
493 To image competition dynamics, fluorescently tagged versions of all relevant strains (Table S2)
494 were pre-cultured and density-adjusted to OD600 = 0.1 as described in 'Competition assays'. For
495 each strain combination, 5 µL were then spotted onto a glass bottom Petri dish filled with 8 mL
496 0.8% w/v LB agar supplemented with 0.5 mM IPTG. After drying for ten minutes at room
497 temperature, the plate was inverted to allow for immediate imaging of the competition area
498 through air. Time-lapse confocal imaging was then carried out using a Zeiss Plan-Apochromat
499 10x objective (NA = 0.45) on a Zeiss LSM880 confocal laser scanning unit using ZEN Black
500 software (version 14.0.18.201). Images (each covering an area of 472.33 µm x 472.33 µm) were
501 acquired hourly for 7 h, over 5 different colony positions, spanning in total the entire radius of the
502 competition area (edge to centre). Three biological replicates were carried out for each strain
503 combination.
504
505 **Confocal image analysis**
506 *Image segmentation and stabilization.* Following acquisition, raw confocal image data were
507 analyzed using FIJI (62). Multichannel images were split into individual channels, with each
508 channel subjected to separate background subtraction (rolling ball radius 50 px) and conversion
509 to binary image data via user-defined thresholds. To maximise the accuracy of cell group
510 boundary tracking, we stabilised images using the FIJI 'StackReg' plugin (64), applied to the GFP
511 (*A. baylyi*) channel. This stabilisation made it necessary to exclude later time points (t = 6,7 h) as
512 these were typically confluent, confounding accurate registration of images. We also excluded
513 colony position 1 (colony edge); here, coffee-ring effects (65) consistently led to the formation of
514 3-D cell groups as early as 2 h into the competition. As our image analysis is limited to 2-D, we
515 were unable to accurately track inter-strain boundaries at this position. For visualization purposes,
516 mtagBFP2 fluorescence is false-coloured orange in all images throughout the manuscript.

517

518 *Inter-strain boundary length (Flank protection).* Beginning with our stabilised, segmented
519 timelapse images, we measured the lengths of *A. baylyi*–EPS- group interfaces by dilating *A.*
520 *baylyi* cell group images (MATLAB *imdilate* method; 3 pixel spherical structuring element),
521 computing their overlap (in pixels) with EPS+ cell groups, and then summing overlapping pixels.
522 We verified that performing this procedure in reverse (dilate EPS- onto *A. baylyi*) yielded similar
523 boundary pixel counts. To account for the greater initial abundance of EPS- cells when EPS+ was
524 absent (2:2 *A. baylyi :* EPS- ratio instead of 2:1:1 *A. baylyi :* EPS- : EPS+), we normalised these
525 boundary measurements by the initial relative abundance of the EPS- strain (that is, dividing
526 interface lengths by 2 for *E. coli* strains growing alone). EPS+ exposure to the attacker was
527 calculated and normalised in the same way.
528 This normalisation likely underestimates the role played by flank protection, because it assumes
529 that a focal strain growing alone with the attacker will start with double the exposure as compared
530 to when it is growing with the other *E. coli* genotype. In reality, the exposure in the single *E. coli*
531 treatments is likely to be less than double, so that the normalisation leads to a lower estimated
532 exposure than reality. To understand why, it is helpful to consider what happens when additional
533 *E. coli* cells are present at the beginning of an experiment. In some cases, these will form
534 independent microcolonies that increase the interface with *A. baylyi*, as our normalisation reflects.
535 However, in other cases these additional *E. coli* cells will simply merge with existing groups
536 instead of growing alone. As a result, starting with more cells will not always proportionally
537 increase attacker exposure. For these reasons, we may underestimate the exposure of *E. coli*
538 growing alone with the attacker. Nevertheless, our measure provides a conservative test of
539 whether flank protection is contributing to cross-protection in experiments, because we still see
540 that exposure of EPS- is reduced by the presence of EPS+.
541

542 *Normalised invasion rates (EPS sharing)*. To estimate T6SS killing rates at inter-strain boundaries
543 (Fig. 4), we tracked changes in strain occupancy at each pixel across consecutive time-lapse
544 images, using custom MATLAB scripts. We compared consecutive time points (t-1, t; t=1,2,3,4,5
545 h) in each stabilised time lapse. Any pixel where EPS- channel signal was lost, and replaced with
546 new *A. baylyi* signal, was marked as being 'invaded' by *A. baylyi*, giving a measure of EPS- cell
547 killing by the attacker. For each time point t, EPS- invasion pixel counts were normalised by the
548 total amount of *A. baylyi*–EPS- contact found in the t-1 image. EPS+ invasion was calculated and
549 normalised in the same way.
550

551 **Statistical Analysis**

552 Statistical analysis and data visualization were performed using RStudio version 1.2.5033 (66)
553 and packages dplyr (67), Rmisc (68), ggplot2 (69), and cowplot (70); as well as Matlab version
554 2017b (9.3.0.713579). For all statistical tests, the significance level α was set to 0.05. To test
555 whether cell recovery differed between competitions (Fig. 2), two-way ANOVA of log-transformed
556 CFU values with a post-hoc Tukey's HSD test was performed. To test whether colanic acid
557 production differed between strains (Fig. S3B), and whether firing rate differed when cells were
558 exposed to EPS (Fig. S4A), a two-sided Wilcoxon rank sum test was performed. To test whether
559 filtering removed EPS from supernatants (Fig. S4B), a two-sided, paired samples Wilcoxon signed
560 rank test was performed. To test whether total attacker exposure or total normalised invasion of
561 the EPS- strain changed when grown alongside the EPS+ strain (or vice versa; Figs. 4D and 4G),
562 we used one-sample Kruskal-Wallis tests. Statistical details (sample size, test values, p-values)
563 for each experiment are provided in the respective figure legends.

564

565 **ACKNOWLEDGEMENTS**

566 We thank Marek Basler, Colin Kleanthous and Frances Spragge for strains, Chris French and
567 Thomas Meiller-Legrand for plasmids, and Erik Bakkeren, Ravinash Krishna Kumar, Jake Palmer,
568 and Rachel Wheatley for comments on the manuscript. We are indebted to Scott Billings and the
569 Oxford Natural History Museum staff, with whom we developed the *GutWars* video game exhibit,
570 for inspiring this project. ETG is funded by a Postdoc Mobility Fellowship from the Swiss National
571 Science Foundation (P400PB_183878) and a BBSRC Discovery Fellowship (BB/V004328/1).
572 WPJS and KRF are supported by the National Institutes of Health (project numbers R01AI093771
573 and R01AI120633), by European Research Council Grant 787932, and by Wellcome Trust
574 Investigator award 209397/Z/17/Z. WPJS is also funded by a Sir Henry Wellcome Postdoctoral
575 fellowship award, 222795/Z/21/Z.

576 **REFERENCES**

577

578 1. M. Ghoul, S. Mitri, The Ecology and Evolution of Microbial Competition. *Trends Microbiol.*
579 **24**, 833–845 (2016).

580 2. M. E. Hibbing, C. Fuqua, M. R. Parsek, S. B. Peterson, Bacterial competition: Surviving
581 and thriving in the microbial jungle. *Nat. Rev. Microbiol.* **8**, 15–25 (2010).

582 3. J. D. Palmer, K. R. Foster, Bacterial species rarely work together. *Science* **376**, 581–582
583 (2022).

584 4. E. T. Granato, T. A. Meiller-Legrand, K. R. Foster, The Evolution and Ecology of Bacterial
585 Warfare. *Curr. Biol.* **29**, R521–R537 (2019).

586 5. S. B. Peterson, S. K. Bertolli, J. D. Mougous, The Central Role of Interbacterial
587 Antagonism in Bacterial Life. *Curr. Biol.* **30**, R1203–R1214 (2020).

588 6. F. R. Cianfanelli, L. Monlezun, S. J. Coulthurst, Aim, Load, Fire: The Type VI Secretion
589 System, a Bacterial Nanoweapon. *Trends Microbiol.* **24**, 51–62 (2016).

590 7. L. P. Allsopp, P. Bernal, L. M. Nolan, A. Filloux, Causalities of War: The connection
591 between T6SS and microbiota. *Cell. Microbiol.*, cmi.13153 (2019).

592 8. P. Bernal, L. P. Allsopp, A. Filloux, M. A. Llamas, The Pseudomonas putida T6SS is a
593 plant warden against phytopathogens. *ISME J.* **11**, 972–987 (2017).

594 9. C. Chen, X. Yang, X. Shen, Confirmed and Potential Roles of Bacterial T6SSs in the
595 Intestinal Ecosystem. *Front. Microbiol.* **0** (2019).

596 10. R. Gallegos-Monterrosa, S. J. Coulthurst, The ecological impact of a bacterial weapon:
597 microbial interactions and the Type VI secretion system. *FEMS Microbiol. Rev.* (2021).

598 11. B. Chassaing, E. Cascales, Antibacterial Weapons: Targeted Destruction in the Microbiota.
599 *Trends Microbiol.* **26**, 329–338 (2018).

600 12. N. Flaugnatti, *et al.*, Human commensal gut Proteobacteria withstand type VI secretion
601 attacks through immunity protein-independent mechanisms. *Nat. Commun.* **12**, 5751
602 (2021).

603 13. S. J. Hersch, *et al.*, Envelope stress responses defend against type six secretion system
604 attacks independently of immunity proteins. *Nat. Microbiol.* **5**, 706–714 (2020).

605 14. S. Robitaille, E. Trus, B. D. Ross, Bacterial Defense against the Type VI Secretion System.
606 *Trends Microbiol.* (2020).

607 15. J. Toska, B. T. Ho, J. J. Mekalanos, Exopolysaccharide protects Vibrio cholerae from
608 exogenous attacks by the type 6 secretion system. *Proc. Natl. Acad. Sci.*, 201808469
609 (2018).

610 16. S. J. Hersch, K. Manera, T. G. Dong, Defending against the Type Six Secretion System:
611 beyond Immunity Genes. *Cell Rep.* **33**, 108259 (2020).

612 17. I. Frost, *et al.*, Cooperation, competition and antibiotic resistance in bacterial colonies.
613 *ISME J.* **12**, 1582–1593 (2018).

614 18. E. T. Granato, K. R. Foster, The Evolution of Mass Cell Suicide in Bacterial Warfare. *Curr.*
615 *Biol.* (2020) (June 5, 2020).

616 19. R. Krishna Kumar, *et al.*, Droplet printing reveals the importance of micron-scale structure
617 for bacterial ecology. *Nat. Commun.* **12**, 857 (2021).

618 20. A. Lopatina, N. Tal, R. Sorek, Abortive Infection: Bacterial Suicide as an Antiviral Immune
619 Strategy. *Annu. Rev. Virol.* **7**, 371–384 (2020).

620 21. D. A. I. Mavridou, D. Gonzalez, W. Kim, S. A. West, K. R. Foster, Bacteria Use Collective
621 Behavior to Generate Diverse Combat Strategies. *Curr. Biol.* **28**, 345-355.e4 (2018).

622 22. D. A. C. Stapels, *et al.*, Salmonella persisters undermine host immune defenses during
623 antibiotic treatment. *Science* **362**, 1156–1160 (2018).

624 23. W. P. J. Smith, *et al.*, Cell morphology drives spatial patterning in microbial communities.
625 *Proc. Natl. Acad. Sci. U. S. A.* **114**, E280–E286 (2017).

626 24. W. P. J. Smith, *et al.*, The evolution of the type VI secretion system as a disintegration
627 weapon. *PLOS Biol.* **18**, e3000720 (2020).

628 25. W. P. J. Smith, *et al.*, The evolution of tit-for-tat in bacteria via the type VI secretion
629 system. *Nat. Commun.* **11**, 5395 (2020).

630 26. H.-C. Flemming, J. Wingender, The biofilm matrix. *Nat. Rev. Microbiol.* **8**, 623–633 (2010).

631 27. H. C. Flemming, S. Wuertz, Bacteria and archaea on Earth and their abundance in
632 biofilms. *Nat. Rev. Microbiol.* **17**, 247–260 (2019).

633 28. B. Lories, *et al.*, Biofilm Bacteria Use Stress Responses to Detect and Respond to
634 Competitors. *Curr. Biol.* **30**, 1231-1244.e4 (2020).

635 29. P. Ghosh, J. Mondal, E. Ben-Jacob, H. Levine, Mechanically-driven phase separation in a
636 growing bacterial colony. *Proc. Natl. Acad. Sci.* **112**, E2166–E2173 (2015).

637 30. J. U. Kreft, J. W. Wimpenny, Effect of EPS on biofilm structure and function as revealed by
638 an individual-based model of biofilm growth. *Water Sci. Technol. J. Int. Assoc. Water*
639 *Pollut. Res.* **43**, 135–141 (2001).

640 31. J. B. Xavier, K. R. Foster, Cooperation and conflict in microbial biofilms. *Proc. Natl. Acad.*
641 *Sci.* **104**, 876–881 (2007).

642 32. A. Berdahl, C. J. Torney, C. C. Ioannou, J. J. Faria, I. D. Couzin, Emergent Sensing of
643 Complex Environments by Mobile Animal Groups. *Science* **339**, 574–576 (2013).

644 33. D. B. Borenstein, P. Ringel, M. Basler, N. S. Wingreen, Established Microbial Colonies
645 Can Survive Type VI Secretion Assault. *PLOS Comput. Biol.* **11**, e1004520 (2015).

646 34. P. D. Ringel, D. Hu, M. Basler, The Role of Type VI Secretion System Effectors in Target
647 Cell Lysis and Subsequent Horizontal Gene Transfer. *Cell Rep.* **21**, 3927–3940 (2017).

648 35. P. N. Danese, L. A. Pratt, R. Kolter, Exopolysaccharide Production Is Required for
649 Development of Escherichia coli K-12 Biofilm Architecture. *J. Bacteriol.* (2000).

650 36. M. Horvat, A. Pannuri, T. Romeo, I. Dogsa, D. Stopar, Viscoelastic response of
651 Escherichia coli biofilms to genetically altered expression of extracellular matrix
652 components. *Soft Matter* **15**, 5042–5051 (2019).

653 37. N. Joshi, B. T. Ngwenya, C. E. French, Enhanced resistance to nanoparticle toxicity is
654 conferred by overproduction of extracellular polymeric substances. *J. Hazard. Mater.* **241–**
655 **242**, 363–370 (2012).

656 38. C. Whitfield, Biosynthesis and Assembly of Capsular Polysaccharides in Escherichia coli.
657 *Annu. Rev. Biochem.* **75**, 39–68 (2006).

658 39. J. van Gestel, F. J. Weissing, O. P. Kuipers, Á. T. Kovács, Density of founder cells affects
659 spatial pattern formation and cooperation in Bacillus subtilis biofilms. *ISME J.* **8**, 2069–
660 2079 (2014).

661 40. M. Rättö, *et al.*, Colanic acid is an exopolysaccharide common to many enterobacteria
662 isolated from paper-machine slimes. *J. Ind. Microbiol. Biotechnol.* **33**, 359–367 (2006).

663 41. C. Sande, C. Whitfield, Capsules and Extracellular Polysaccharides in Escherichia coli and
664 Salmonella. *EcoSal Plus* **9**, eESP-0033-2020 (2021).

665 42. M. M. Hahn, J. S. Gunn, Salmonella Extracellular Polymeric Substances Modulate Innate
666 Phagocyte Activity and Enhance Tolerance of Biofilm-Associated Bacteria to Oxidative
667 Stress. *Microorganisms* **8**, 253 (2020).

668 43. J. Chen, S. M. Lee, Y. Mao, Protective effect of exopolysaccharide colanic acid of
669 Escherichia coli O157:H7 to osmotic and oxidative stress. *Int. J. Food Microbiol.* **93**, 281–
670 286 (2004).

671 44. T. Ophir, D. L. Gutnick, A role for exopolysaccharides in the protection of microorganisms
672 from desiccation. *Appl. Environ. Microbiol.* **60**, 740–745 (1994).

673 45. K. Mizoguchi, *et al.*, Coevolution of Bacteriophage PP01 and Escherichia coli O157:H7 in
674 Continuous Culture. *Appl. Environ. Microbiol.* **69**, 170–176 (2003).

675 46. P. D. Scanlan, A. Buckling, Co-evolution with lytic phage selects for the mucoid phenotype
676 of Pseudomonas fluorescens SBW25. *ISME J.* **6**, 1148–1158 (2012).

677 47. S. Wielgoss, T. Bergmiller, A. M. Bischofberger, A. R. Hall, Adaptation to Parasites and
678 Costs of Parasite Resistance in Mutator and Nonmutator Bacteria. *Mol. Biol. Evol.* **33**,
679 770–782 (2016).

680 48. P. Domenico, R. J. Salo, A. S. Cross, B. A. Cunha, Polysaccharide capsule-mediated
681 resistance to opsonophagocytosis in Klebsiella pneumoniae. *Infect. Immun.* **62**, 4495–
682 4499 (1994).

683 49. T. A. Russo, *et al.*, The K1 capsular polysaccharide of Acinetobacter baumannii strain 307-
684 0294 is a major virulence factor. *Infect. Immun.* **78**, 3993–4000 (2010).

685 50. M. R. Wessels, A. E. Moses, J. B. Goldberg, T. J. DiCesare, Hyaluronic acid capsule is a
686 virulence factor for mucoid group A streptococci. *Proc. Natl. Acad. Sci.* **88**, 8317–8321
687 (1991).

688 51. C. D. Nadell, K. Drescher, K. R. Foster, Spatial structure, cooperation and competition in
689 biofilms. *Nat. Rev. Microbiol.* **14**, 589–600 (2016).

690 52. N. M. Oliveira, R. Niehus, K. R. Foster, Evolutionary limits to cooperation in microbial
691 communities. *Proc. Natl. Acad. Sci. U. S. A.* **111**, 17941–17946 (2014).

692 53. S. Mitri, J. B. Xavier, K. R. Foster, Social evolution in multispecies biofilms. *Proc. Natl.*
693 *Acad. Sci. U. S. A.* **108**, 10839–10846 (2011).

694 54. M. Raffatellu, Learning from bacterial competition in the host to develop antimicrobials.
695 *Nat. Med.* **24**, 1097–1103 (2018).

696 55. C. Rüter, P. R. Hardwidge, 'Drugs from Bugs': bacterial effector proteins as promising
697 biological (immune-) therapeutics. *FEMS Microbiol. Lett.* **351**, 126–132 (2014).

698 56. G. Corno, K. Jürgens, Direct and Indirect Effects of Protist Predation on Population Size
699 Structure of a Bacterial Strain with High Phenotypic Plasticity. *Appl. Environ. Microbiol.* **72**,
700 78–86 (2006).

701 57. R. M. Donlan, J. W. Costerton, Biofilms: Survival Mechanisms of Clinically Relevant
702 Microorganisms. *Clin. Microbiol. Rev.* **15**, 167–193 (2002).

703 58. A. Schulze, F. Mitterer, J. P. Pombo, S. Schild, Biofilms by bacterial human pathogens:
704 Clinical relevance – development, composition and regulation – therapeutical strategies.
705 *Microb. Cell* **8**, 28–56 (2021).

706 59. M. Jamal, *et al.*, Bacterial biofilm and associated infections. *J. Chin. Med. Assoc. JCMA*
707 **81**, 7–11 (2018).

708 60. S. Galié, C. García-Gutiérrez, E. M. Miguélez, C. J. Villar, F. Lombó, Biofilms in the Food
709 Industry: Health Aspects and Control Methods. *Front. Microbiol.* **9** (2018).

710 61. T. J. Rudge, P. J. Steiner, A. Phillips, J. Haseloff, Computational modeling of synthetic
711 microbial biofilms. *ACS Synth. Biol.* **1**, 345–352 (2012).

712 62. J. Schindelin, *et al.*, Fiji: An open-source platform for biological-image analysis. *Nat.*
713 *Methods* **9**, 676–682 (2012).

714 63. B. Obadia, *et al.*, Influence of Tyrosine-Kinase Wzc Activity on Colanic Acid Production in
715 Escherichia coli K12 Cells. *J. Mol. Biol.* **367**, 42–53 (2007).

716 64. P. Thevenaz, U. E. Ruttimann, M. Unser, A pyramid approach to subpixel registration
717 based on intensity. *IEEE Trans. Image Process.* **7**, 27–41 (1998).

65. A. Agrawal, S. Sinha, R. Mukherjee, D. Mampallil, Dynamics of bacterial deposition in evaporating drops. *Phys. Fluids* **32**, 093308 (2020).

66. R Development Core Team, *R: A language and environment for statistical computing.* (R Foundation for Statistical Computing, 2018).

67. L. H. and K. M. Hadley Wickham, Romain François, dplyr: A Grammar of Data Manipulation. R package version 0.7.6 (2018).

68. R. M. Hope, Rmisc: Ryan Miscellaneous. R package version 1.5. (2013).

69. P. M. Valero-Mora, *ggplot2: Elegant Graphics for Data Analysis* (Springer, 2010).

70. C. O. Wilke, cowplot: Streamlined Plot Theme and Plot Annotations for “ggplot2”. R package version 0.9.4. (2019).